SLAC – PUB – 4457
October 1987
(T/E)

REPORT OF THE NON-MAGNETIC DETECTOR GROUP*

T. Åkesson† and C. W. Fabjan
CERN, CH-1211 Genève 23, Switzerland
R. N. Cahn, C. Klopfenstein, R. J. Madaras, M. T. Ronan,
M. L. Stevenson, M. Strovink,† and W. A. Wenzel
Lawrence Berkeley Laboratory, Berkeley, California 94720
J. M. Dorfan‡ and G. J. Feldman†
Stanford Linear Accelerator Center, Stanford University, Stanford, California 94305
P. Franzini and P. M. Tuts‡
Columbia University, New York, New York 10027
D. Hedin‡
Northern Illinois University, Dekalb, Illinois 60115
C. A. Heusch
University of California, Santa Cruz, California 95064
M. D. Marx
State University of New York, Stony Brook, New York 11794
H. P. Paar‡
University of California, La Jolla, California 92093
F. E. Paige and S. D. Protopopescu
Brookhaven National Laboratory, Upton, New York 11973
R. Raja
Fermi National Accelerator Laboratory, Batavia, Illinois 60510
P. G. Rancoita
INFN, I-20133 Milano, Italy
D. D. Reeder‡
University of Wisconsin, Madison, Wisconsin 53706
J. S. Russ‡
Carnegie-Mellon University, Pittsburgh, Pennsylvania 15213
J. P. Rutherfoord
University of Washington, Seattle, Washington 98195
L. R. Sulak and J. S. Whitaker‡
Boston University, Boston, Massachusetts 02215
A. P. White‡
University of Florida, Gainsville, Florida 32611

* Work supported in part by the Department of Energy, contracts DE–AC03–76SF00515 and DE–AC03–76SF00098.
† Group coordinator
‡ Subgroup coordinator

To appear in the Proceedings of the Workshop on Experiments, Detectors, and Experimental Areas for the Supercollider, Berkeley, California, July 7–17, 1987

1. Introduction: Why a Non-Magnetic Detector?

Why should anyone consider a non-magnetic detector for the SSC? Other things being equal, a detector does not improve by removing a feature.

The question in this case is whether the requirement of measuring the momenta of 1 TeV/c electrons hinders higher priority goals, such as optimum calorimetry. The orientation of the non-magnetic group is that calorimetery and lepton detection are the most important characteristics of an optimized SSC detector. Thus, a "non-magnetic" detector does not necessarily mean the absence of a magnetic field in any particular region; it merely means that the magnetic field does not play a major role in the optimization of the detector.

What are the direct physics advantages of magnetic analysis? At the parton level, the only advantage is a determination of the electron sign. (In any detector, the sign of the muon will be determined by magnetic analysis and the sign of a quark jet is not measurable.) There were only a few physics processes reported to us by the parameterization groups which benefited from a central magnetic field. These were like-sign W pair production and asymmetry measurements from new W and Z bosons. In both cases the physics can be done with muons alone at a cost of two or four in rate.

Are there other advantages to having a central magnetic field? We considered several possibilities which are listed below with comments:

1. Redundancy: The argument is that cracks or inefficiencies in calorimeters can be found by seeing stiff tracks pointing to them. This argument is based on experience with present day "hermetic" detectors. Considering the precision required by SSC calorimeters and the fact that approximately half of all energy is carried by neutral particles, we do not find this a compelling argument in the SSC environment. Calorimeters with cracks or inefficiencies large enough to make this redundancy check useful at the SSC will simply be incapable of measurements of adequate precision.
2. Secondary vertex detection: Secondary vertex detectors will not work without some level of momentum measurement because there will be too much confusion from multiple scattering of soft particles. A modest magnetic field which might be inserted into a "non-magnetic" field would probably be sufficient for this purpose. However, the usefulness of secondary vertex detection for high-p_t physics seems minor:
   (a) b Jets: Monte Carlo simulations have shown that on the average, every 500 GeV/c p_t jet has a fairly stiff B meson in it. Thus, at high p_t the identification of a b jet does not seem to be a very powerful signature.
   (b) τ's: In almost all cases, τ's will be lost in the multihadronic jet background. In cases in which the τ is well isolated, most physics process will also yield electrons and muons, which can be identified with higher efficiency.
3. p/E for electron identification: This is probably useful, but we are not sure to what extent. We will return to this point when we discuss electron identification.

2. The Detector

Table 1 shows a list of requirements for a non-magnetic detector that match well the needs specified by the physics subgroups.

Table 1: Detector Requirements

Electrons:	$\|y\| \leq 3$
	$\Delta E/E \leq 15\%/\sqrt{E}$
	$\Delta E/E \leq 1\%$ (systematic)
	hadron misidentification $\ll 10^{-3}$
Muons:	$\|y\| \leq 3$
	$\Delta p/p \approx 13\%$ at 1 TeV
Calorimetry:	$\|y\| \leq 5.5$ for hermeticity
	$\|y\| \leq 3$ for jet reconstruction
	$\Delta y = \Delta\phi \approx 0.05$ (hadronic towers)
	$\Delta E/E \leq 50\%/\sqrt{E}$
	$\Delta E/E \leq 2\%$ (systematic)
	hermetic design

Figure 1 shows a schematic drawing of the detector which we are proposing to meet the requirements listed above. In the next three sections, we will discuss the methods we propose to achieve the necessary calorimetry and lepton identification.

3. Tracking and Election Identification

As outlined in this section, we will accomplish charged-particle tracking and electron identification using transition radiation detectors (TRD's) in one compact device. It will be placed inside the calorimeter and will cover ± 3 units of rapidity. To cover this large rapidity range requires dividing the tracking volume into several geometrical regions — the central (or barrel) region and the forward regions — each requiring appropriate resolution. The exact placement of the transition between these regions and the best choice of coordinates for each region requires a careful study of structural integrity, readout, and minimization of dead space. In the absence of a detailed design we have chosen the representative set of parameters given below.

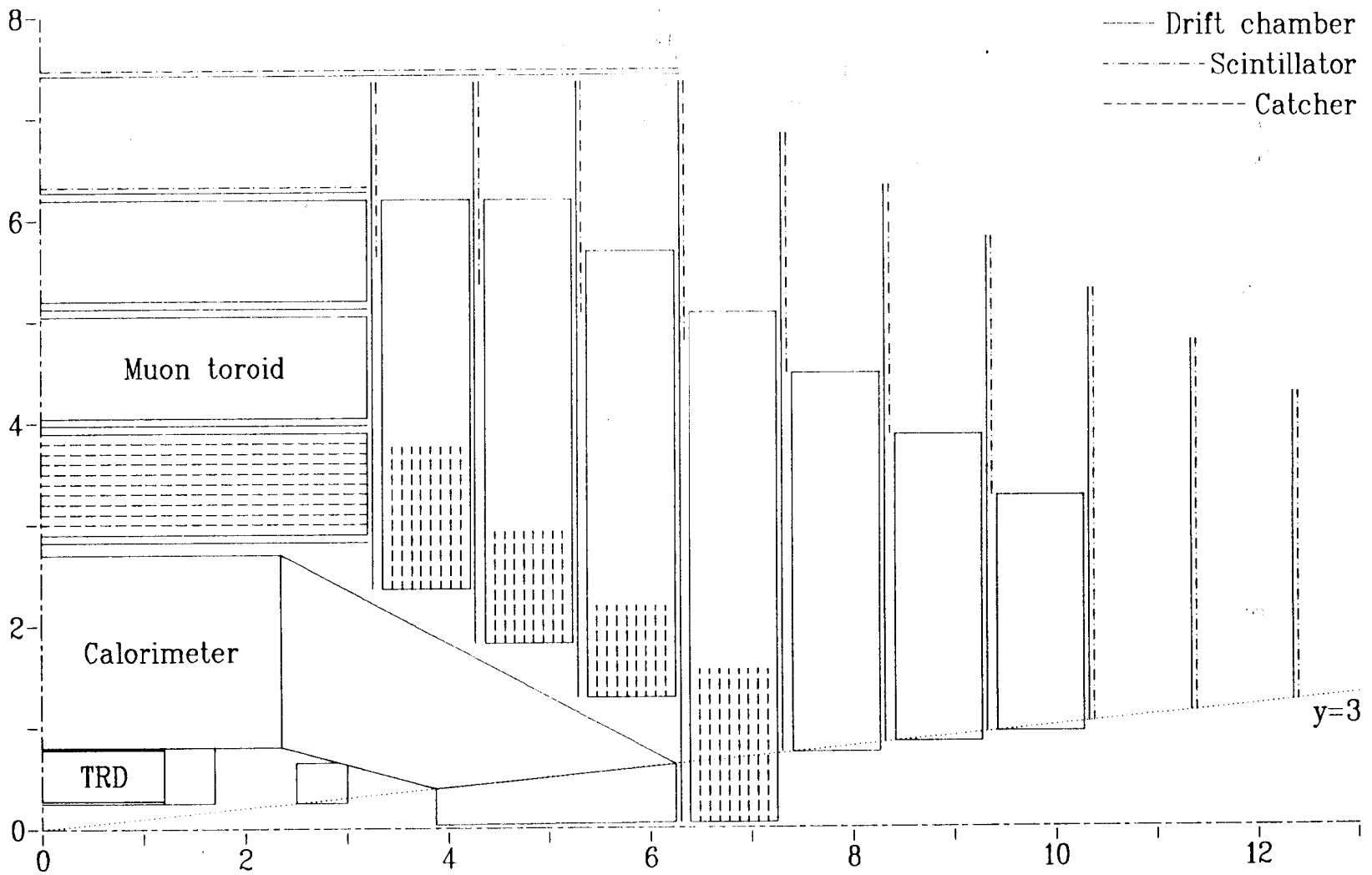

11-87

5891A16

Fig. 1a. Elevation View of the "Non-Magnetic Detector."

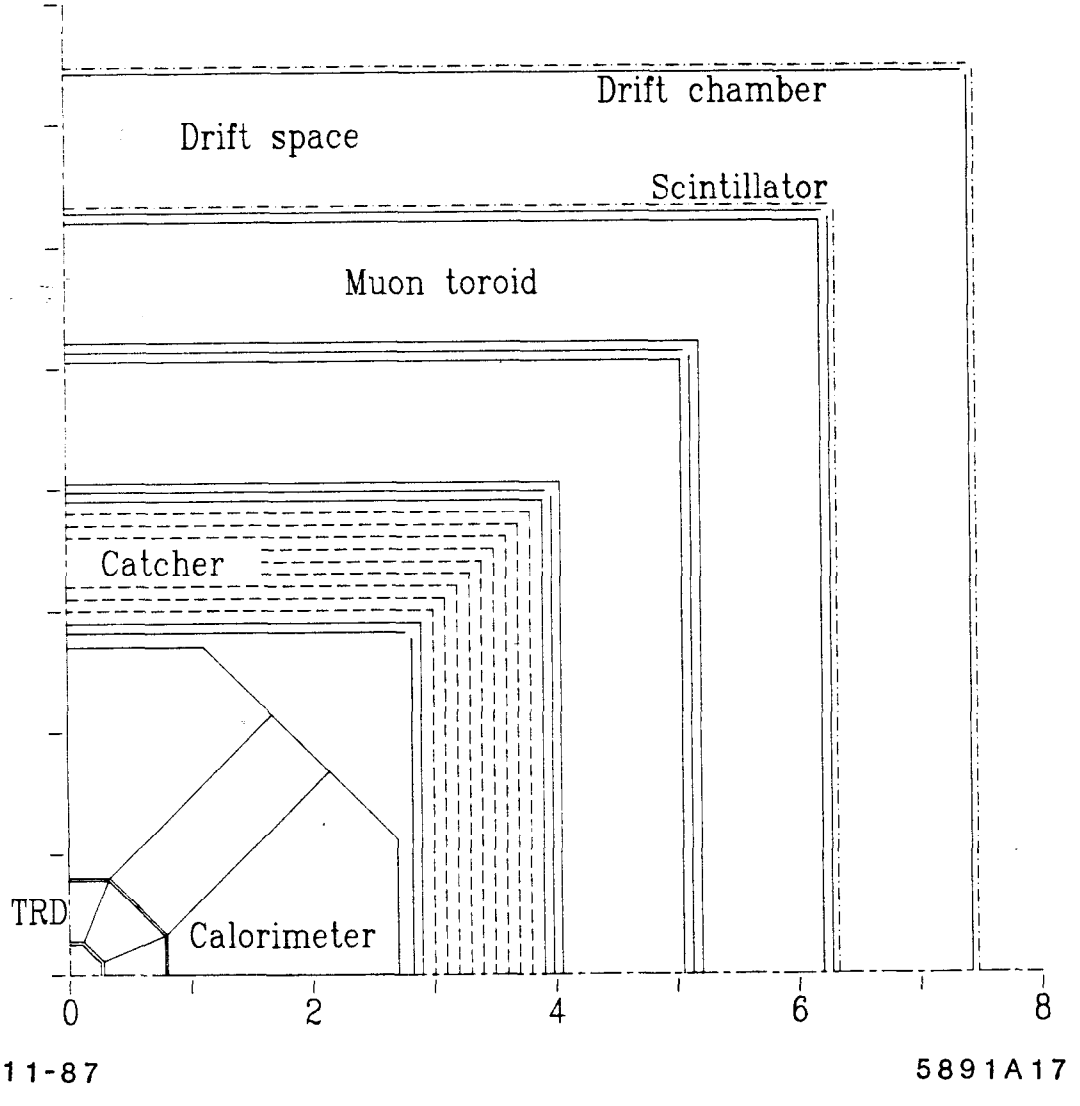

Fig. 1b. Cross Sectional View of the "Non-Magnetic Detector."

3.1. Tracking Considerations

The main functions of charged particle tracking in a non-magnetic detector are:

1. The measurement of the longitudinal position of the event vertex, which helps resolve the event overlap problem and improves muon momentum measurement.
2. The ability to project charged tracks into the calorimeter and thereby eliminate fake electrons which arise from hadron/photon overlap.

If in addition one adds a central magnetic field to the tracking system, one can further achieve:

3. Charged particle momentum measurement which provides redundancy with respect to the calorimeter measurements.
4. Additional hadron/electron rejection from the p/E match criterion.
5. Determination of the sign of electrons.

However, there are counterbalancing arguments which must be considered before adding a magnetic field. These include space, engineering and performance compromises made to accommodate the coil, the possible limitations placed on the calorimetry transducers (phototubes or transformer coupled readout), confusion for the tracking system from particles which are trapped by the field, and physical separation of $e^{\pm}$ from photon conversions which might result in additional backgrounds to prompt $e^{\pm}$ signals.

None of the benefits of the magnetic field seemed compelling to the non-magnetic detector group, but with more careful evaluation it might become desirable. Simulations are needed to establish how bad the track confusion problems are and to what extent, if any, hadron/electron separation is enhanced by the p/E match given that the detector will have excellent calorimetry, track pointing, and TRD's. The tentative conclusion then would be not to exclude the possibility of providing a moderate ($\approx$5 KG), warm coil, but to make sure that retaining this possibility does not become a major driving force in the detector design. Referring to Fig. 1, one sees that such a coil could fit naturally into the space between the precision calorimeter and the tail catcher, following the external shape of the precision calorimeter.

3.2. Electron Identification with TRD's

Efficient identification of electrons will be the key to much of the most interesting physics at the SSC. Background to electron identification in the SSC environment will arise both from single hadrons and from jets. The pattern of calorimetric energy deposition can provide single pion rejection in the range 10^{-2} to 10^{-3} depending on sampling granularity.[1] Tracking charged particles and comparing the extrapolated track with the centroid of electromagnetic energy deposition in the calorimeter will augment pion rejection. Additional independent electron identification systems will likely be required to beat down the backgrounds that arise in the study of isolated electrons, and, in the study of electrons in jets, from the limitations of calorimeter granularity and large multiplicity. A

transition radiation detector (TRD) will provide additional pion rejection on a per track basis. The TRD in an SSC detector primarily will reject fake electron candidates that are selected by calorimetric criteria.

3.3. A Straw Design

In the present design the TRD and tracking functions are integrated in a straw wire chamber system.[2] This system will provide charged particle tracking to rapidity of 3. It will identify electrons with high efficiency and by itself will have pion rejection of better than 10^{-2}.

The design is shown in Fig. 2. The solid angle is divided into three regions: the central region, $|z| < 120$ cm; the forward region, 120 cm $< |z| <$ 170 cm; and the very forward region, 250 cm $< |z| <$ 300 cm. In each region there are 32 repetitions of a basic TRD unit. The TRD unit consists of 1 cm of radiator and two layers of straw chambers in close packing. The total thickness of a TRD assembly is 50 cm.

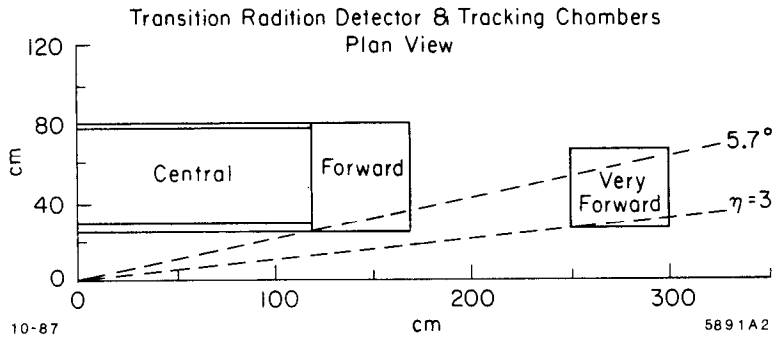

Fig. 2. Plan view of the transition radiation detector and tracking system.

In the central region, the TRD radiators form hexagonal cylinders with sides parallel to the z axis. The straw chambers form hexagonal "cobwebs" in the x-y plane. This geometry reduces the occupancy of each wire to an acceptable level and provides good dip angle measurement. The TRD occupies 28 cm $< r <$ 78 cm. Inboard from the TRD there are eight layers of straws running axially, at radius 25 to 28 cm. Outboard from the TRD are four more layers of axial straws.

In the forward and very forward regions, the TRD radiators form planes that are perpendicular to the z axis. Each TRD consists of a 50 cm package of 32 TRD units as in the central region. The straw chambers also lie in the x-y plane. They are arranged in parallel arrays; successive planes are rotated by 60° to give stereo information for track reconstruction. The forward region occupies 25 cm $< r <$ 80 cm and the very forward region occupies 25 cm$< r <$ 65 cm. The total system provides TRD coverage to $|\eta| = 3$.

This design incorporates a very large number of straw chambers. The straw diameter is set at 4 mm as part of the optimization of the TRD performance. In the TRD there are approximately 230,000 straws in the central region, 35,000 in each forward region, and 32,000 in each very forward region. The total number of TRD straws is 364,000. The axial straws number roughly 17,000, assuming that 240 cm long straws are feasible.

3.4. Tracking System

In the central region, charged particles are tracked in the r-ϕ plane by the axial straws and in the r-z plane by the TRD straws. The axial straws are equipped with charge division readout and multiple hit electronics to allow a match with tracks in the TRD. Particles at $\theta > 30°$ will be projected into the calorimeter with resolution of order 1 mm in both azimuthal and longitudinal directions. In the forward angles ($5° < \theta < 30°$) the 32 y-u-v measurements from the TRD straws (see below) will provide comparable resolution.

3.5. TRD Implementation

Transition radiation detectors can be operated in two different modes: total ionization measurement and cluster counting.[3] In the first case the TRD is optimized for high energy X-rays and one measures in the X-ray absorption gap the combined signal of ionization and X-rays. The Landau-distributed fluctuations in dE/dx diminish the electron identification power of the TRD. The second method counts the number of energy deposits above a given threshold. In this case one measures the transition radiation quanta in a large number of proportional chambers sensitive to low energy X-rays. The thickness of each proportional chamber is sufficiently small that the typical ionization energy deposition is significantly smaller than the energy deposition from an X-ray interaction. The identification power of the TRD in this case depends on the Poisson-distributed number of δ-rays. The smaller fluctuations in the Poisson distribution relative to the Landau distribution can give the cluster-counting method better controlled tails and better pion rejection.

The present design is based on the cluster counting method. The radiator is optimized for production of X-rays with energies around 5 keV by controlling the fiber diameter and packing.[4] The radiator is divided into 1 cm slabs, each followed by a double layer of straws. This radiator thickness is roughly equal to the X-ray attenuation length. This arrangement of the straws provides numerous uncorrelated samples for the measurement of the X-ray production probability and is well suited to their simultaneous use in charged particle tracking.

The straw chambers are filled with a xenon-rich gas mixture to enhance X-ray detection efficiency. The walls of the straws are thin enough that X-ray absorption is negligible compared to interactions in the gas. Straws of polycarbonate and mylar with 30 μm walls have been achieved;[5] these walls are just a few per cent of the X-ray absorption length. In a gas that is 60% xenon, the X-ray interaction probability in the double layer

of straws is approximately 80%. For a high energy electron, there will be approximately 1/4 detected X-ray per double layer of straws.[3] The energy deposited by ionization by the primary particle is 2 keV per layer, a fraction of the energy deposited in the gas by a typical X-ray interaction.

Given the large number of straw chambers, the electronics per straw must be simple and inexpensive. One possibility is to use "two-bit" electronics: each straw would be instrumented with one channel consisting of an amplifier and two comparators along with associated readout. A low threshold would be used to flag the low energy deposit from the primary particle ionization; a higher threshold being exceeded would flag an X-ray interaction.

3.6. TRD Test Results

A detector similar to the present design has been described in Ref. 3. The detector, shown in Fig. 3, consists of a large number of radiator-proportional chamber sets. Each radiator has a length of 1 cm and consists of 40 polypropylene foils with a thickness of 18 μm each. The proportional chamber is 3 mm thick and has a wire spacing of 2 mm. The chamber gas is a mixture of 60% xenon, 35% helium, and has 5% methane as a quencher.

The single-particle response of such a detector is shown in Fig. 4. The relevant figure of merit is the rejection factor R, defined as the ratio of pion efficiency to electron efficiency. Figure 4(a) shows R versus detector length for a 50 GeV particle when 90% electron efficiency is required. Figure 4(b) shows the variation of rejection with particle energy for a 40 cm long detector with 30 proportional gaps. The number of clusters required for an electron signal corresponds to 90% electron efficiency at 50 GeV. The rejection has a minimum of 2×10^{-3} at 3 GeV and then rises slowly until about 200 GeV where the pions start radiating. The slow rise until 200 GeV is due to increased δ-ray production by the pions. Poor rejection below 3 GeV is due to the drop in electron efficiency. The excellent rejection of low energy pions will provide the improvement in electron identification necessary to supplement the calorimetric response.

3.7. TRD Performance in Jets

The performance of the detector described in the previous section has been simulated using ISAJET.[6] The geometry assumed 2-meter axial wires starting at 20 cm from the beam axis, so the results will be a "worst-case" bound on the performance of the present design. Two-jet events at 500 GeV per jet were generated assuming one interaction per beam crossing. Figure 5(a) shows the number of charged particles per azimuthal segment per event versus the azimuthal angle from the jet axis. An azimuthal segment is the angle subtended by one proportional cell at 20 cm radius, or 0.6° for the test detector. The level varies from 0.7 at the jet axis to 0.2 at 45° from the jet. The properties of the particles vary strongly over this region. This is clearly demonstrated in Fig. 5(b), which plots the probability per jet and per azimuthal segment that the hadrons fake an electron, requiring 90% electron efficiency. The distribution has a level of about 10^{-3} for angles

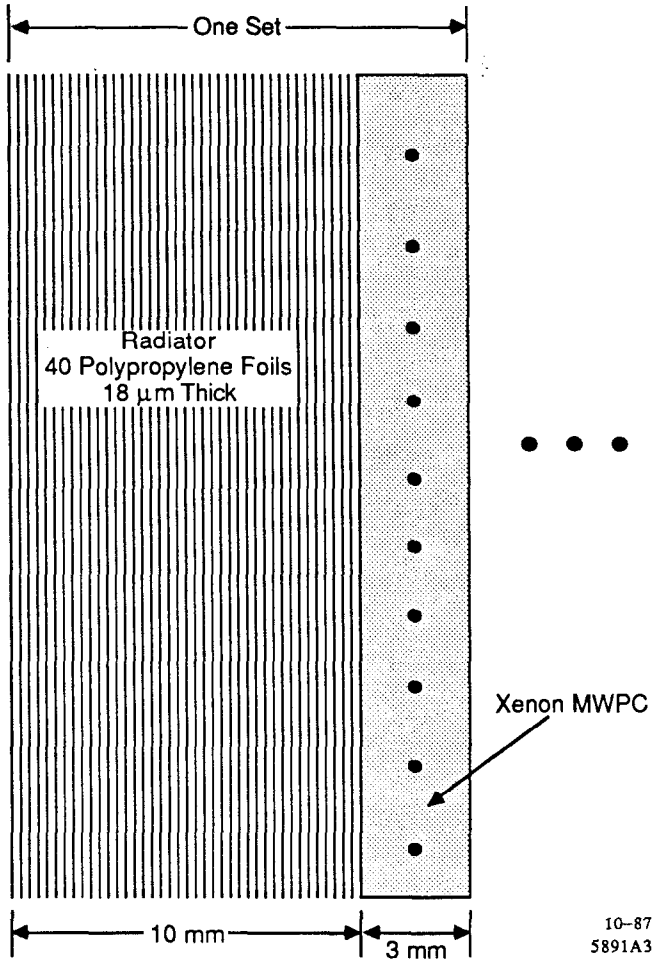

Fig. 3. Configuration of the test detector in Ref. 3.

larger than 5° from the jet axis and rises to about 15% at the jet core. The reason for this increase is twofold: the pions are energetic and start to radiate, and they have, of course, a strong angular correlation. Considering the role of the TRD response as a test of electron candidates selected calorimetrically, Fig. 5(b) demonstrates a TRD rejection factor of 1000 as close as 5° from the jet axis.

This same ISAJET study was used to estimate the effect on wire chamber performance of radiation from beam-beam interactions. Using data on gain shift versus integrated charge given by Walenta,[7] the innermost axial wire in the tracking system should experience a gain change of only about 5% in a year of running at the nominal luminosity of 10^{33} $cm^{-2}s^{-1}$.

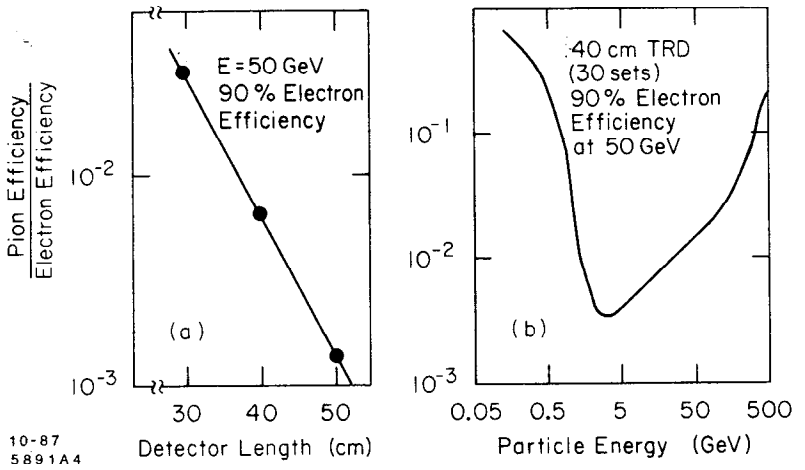

Fig. 4. (a) Rejection at 50 GeV versus TRD length. (b) Rejection for the 40 cm test TRD versus particle energy. From Ref. 3.

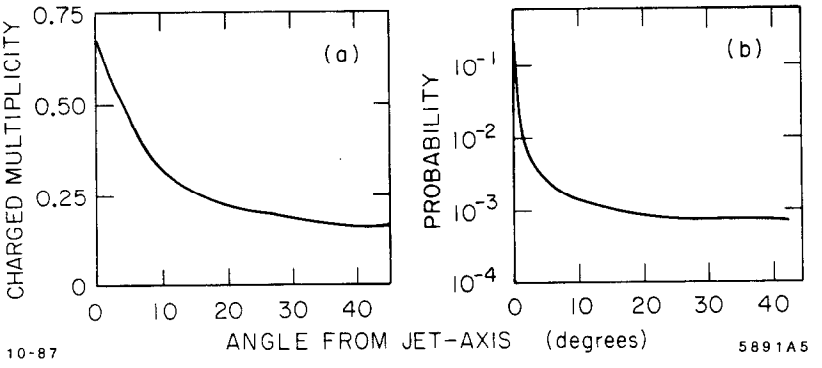

Fig. 5. (a) Number of charged particles per azimuthal segment and per jet versus azimuthal angle from jet axis, for 500 GeV ISAJET jets. (b) Probability per azimuthal segment and per jet that charged hadrons fake an electron, versus angle from the jet axis.

4. Calorimetry

4.1. Introduction

The design discussion for the non-magnetic detector calorimetry benefitted greatly from the experience gained on current detectors and prototypes, and particularly from recent work on the detailed understanding of the role of compensation in determining calorimeter performance.[8] This experience and understanding were applied to the evaluation of a variety of possible calorimeter designs for the SSC. Some designs have already received much attention at other workshops, but newer, innovative approaches were also

considered. Because a large number of questions were raised, many of which need R&D or engineering studies to answer, it was not possible to make a specific recommendation for a calorimeter technique. The following sections therefore contain detailed consideration of a number of options, and comparative discussion.

The physics requirements for the calorimetry as defined by the physics subgroups have been summarized in Table 1. We begin below with a discussion of the additional operational requirements that any calorimeter at the SSC must satisfy. We then discuss the general calorimeter design in the context of the non-magnetic detector as a whole system. This is followed by detailed examination of a number of proposed techniques which represents the main part of the subgroup's activities. We then give a critical comparison of these techniques and end by listing questions and topics for future R&D.

4.2. Operational Requirements

There are a number of requirements that must be satisfied by any calorimeter system and some that arise specifically from the environment of an SSC experiment. Most of these requirements are not unique to the non-magnetic detector but were discussed in detail and form much of the basis for our critical comparisons later. Further, this list of requirements is not exhaustive but reflects the main areas of concern of the members of the subgroup.

4.2.1. Radiation hardness

It has been calculated that the radiation dose at the face of an SSC calorimeter will vary from 10^3 rads/year at η =0 to 10^{10} rads/year in the η >5.5 region at the 10^{33} design luminosity.[9] Depending on the design, the active calorimeter material, readout path, and electronics are all potentially at risk from this radiation. The resulting problems can be complex. In a piece of scintillator or scintillating fiber, the matrix, fluor, and wavelength shifter can all be damaged, resulting in changing efficiencies for light production, transmission, and output. The detailed study and separation of such effects is only now being undertaken in conjunction with the search for more radiation resistant media.

Apart from the direct radiation from the interaction point, there are also large numbers of neutrons produced in the passive material, particularly when this material has a large atomic weight (*e.g.*, uranium). The magnitude of this effect has only recently been estimated.[10] In view of this incomplete knowledge of radiation effects, it is not possible to give a definitive statement on the survival time of certain calorimeter materials beyond optimistic extrapolation from present knowledge. However, for some of the more radiation sensitive techniques it is already apparent that the high radiation regions at low polar angle will require a change in technology that could potentially introduce strange effects across boundaries.

4.2.2. Calibration and Stability

It is a fundamental requirement to be able to calibrate the calorimeter and know over what period it will be stable, so as to give a contribution to the energy resolution which

is small compared to other unavoidable contributions. Sources of instability can lie in variations in active material density and purity (liquids), radiation damage effects, and drifts in electronics. To achieve a good calibration it must be possible to monitor each part of the calorimeter and readout path since, for instance, radiation effects will vary with polar angle and depth into the calorimeter. While it is relatively easy to arrange for testing of the readout path even with amplifiers mounted on the calorimeter, it is much more difficult, particularly in certain designs, to arrange to be able to create calibration "energy" deposits throughout the active volume of the calorimeter.

4.2.3. Speed of Response

The problems of calorimeter pile-up effects due to the high event rate at the SSC were examined quantitatively at Snowmass 86.[11] For cases in which the integration time is long compared to the beam crossing interval, significant residual energy ("physics noise") and missing E_t contributions can result. Generally the magnitude of such effects was found to depend on the square root of the signal development time. Thus an increase in the drift velocity of a liquid by a factor of two may be insufficient. Clearly, the best solution is to use an intrinsically fast response device.

4.2.4. Hermeticity

Much of the new physics predicted for the SSC requires the ability to be confident that a significant amount of energy has not been lost in a dead region of the detector. While any initially hermetic calorimeter design will become modified by the realities of structural engineering, some options are intrinsically less problematic in this area. However, there is still room for imaginative new approaches to the location of dead regions in established techniques. Careful and detailed simulation is needed, for instance, to decide the relative merits of a scheme with one major but thoughtfully situated dead region and a scheme with more uniformly distributed but individually less significant dead spots.

4.2.5. Calorimeter Depth and Shower Containment

The parametrization of Gordon and Grannis indicates that a calorimeter should have a depth of 10 $\pm$1 interaction lengths in order to contain a 1 TeV hadron shower at the 98% level.[12] The remaining few percent should be measured in several more interaction lengths of coarse "tail catcher" calorimetry to ensure a low level of energy leakage.

4.2.6. Electron Identification

Good transverse and longitudinal segmentation is required to provide hadron rejection and allow for electron isolation for decay tagging.

4.3. General Design

Given the absence of a magnetic field and the consequent removal of the need for long track lengths for momentum reconstruction, one can consider a compact calorimeter design to surround the limited volume of the TRD-tracker system. The inner radius of the calorimeter was thus set to be 0.8 meter.

The general approach to the calorimeter design was to use an adequately compensated "fine" calorimeter 8 to 9 interactions lengths deep, backed by a 4 to 5 interaction length magnetized iron tail catcher which also forms the first part of the muon system. The catcher would typically measure about 2% of the energy in a 1 TeV shower and can thus afford to be a device of inferior resolution. A significant cost saving is also achieved by the resulting limitation on the outer radius of the "fine" calorimetry.

The fine calorimeter has an electromagnetic section with three longitudinal segments, the second segment having a finer transverse segmentation than the others for improved electromagnetic shower position measurement. There is also the option in some designs to install a very fine position measurement detector behind the second segment to distinguish electrons from nearby photon showers. The fine hadronic calorimetry also has three longitudinal segments.

The general shape of the calorimeter has three main features, a barrel section, a sloping end section and a low polar angle plug section (Fig.1). The sloping end section gives an approximately uniform angle of incidence over its length for particles from the interaction region, and allows larger physical tower sizes (of fixed rapidity interval) at the lower angles than would an orthogonal end cap situated at the end of the barrel section.

In the low polar angle region we have avoided a scheme with a disconnected forward calorimeter since studies for D0 have shown that such an arrangement gives a worse missing-p_t resolution.[13]

4.4. Specific Techniques

Four possible techniques were considered in detail:

(a) Lead (or uranium)/liquid argon

(b) Lead (or uranium)/warm liquid

(c) Uranium/silicon

(d) Lead/scintillating fibers

The liquid argon option is by now a reasonably well understood technique although with potentially serious drawbacks in terms of dead areas that would require a very careful engineering study for the SSC. The alternative of using a warm liquid, which may go a long way towards solving the hermeticity problems, has been the subject of much recent development but a great deal still remains to be learned about actual operational use.

If a compact calorimeter design is possible then the third option of using silicon as the active medium becomes financially viable, although there are many unknowns since such a device has only been tested as an electromagnetic calorimeter; a hadronic prototype is still under construction.

The last option, lead/scintillating fibers, is the most speculative, but potentially offers the possibility of constructing a high performance calorimeter if questions of segmentation, calibration and radiation sensitivity can be satisfactorily resolved.

We shall now consider each of these options in detail. The degree of detail for the various designs varies according to factors such as the amount of prior work performed, the level of attention received at the Workshop, and the desire to avoid repeating well known facts about the more established approaches.

4.4.1. Lead (Uranium)/Liquid Argon

Of all the choices for sampling calorimetry at the SSC, liquid argon provides the best developed and understood choice. For this option we did not evolve a specific design as was done for the other options discussed below. We describe here only the main point of concern about liquid argon which was discussed at the Workshop.

While the understanding of liquid argon calorimetry extends to its inherent advantages (stability, radiation hardness, and signal size (relative to warm liquids), its disadvantage, as displayed in current experiments like D0, is also clearly indicated. This disadvantage is the lack of hermeticity introduced by segmenting the calorimetry into 3 angular intervals, each contained in its own double-walled insulation vessel.

In D0 this is the region between central and endcap calorimeters as shown in Fig 6. Both the endcap and central calorimeter vessels are made of stainless steel. This choice was dictated primarily by the desire to have code vessels which are welded closed after insertion of the calorimeter modules. The choice of welded vessels was dictated by both monetary and space constraints, as well as a prejudice against the complexity of cryo-liquid seals. It should be noted, that of the inert material in this transition region, almost one half comes from the support mechanisms for the calorimeter modules. This amount of material is likely to occur in any calorimeter — warm liquid, scintillator/lead, etc. — for support columns and for readout and access channels.

Another design for this transition region is shown in Fig. 7, the vessel designed for the H1 liquid-argon calorimeter at HERA.[14] This design makes use of the e-p kinematics, requiring hermeticity only in the proton direction. The single vessel encompasses both the central and endcap regions. In addition the vessel walls between tracking and calorimetry are aluminum, while the remainder of the vessel is stainless steal. Finally, the vessel is sealed using flanges and sliding seals between dissimilar metals. An additional complication in this design are the support feet, which must accommodate the 0.3% relative motion of the warm and cold vessels. Approximately four times more engineering resources were applied to the design of the H1 vessel than the D0 vessel.

Designs of liquid argon calorimetry for the SSC will have to further optimize the arrangement of modules and vessel designs. One can clearly make the design of a liquid argon system competitive with other choices (warm liquid, lead/scintillator) by placing the entire system within one large vessel. Since, as in the H1 design, the inner vessels can be aluminum, this design would be indistinguishable from other systems from the point of hermeticity. However, complications from this approach arise because the tracking system is sealed within the interior volume. One must solve the problems of cables and services, which can be accomplished with re-entrant holes through the calorimeter volume, and access to the tracking system. A possible solution is to build a "NASA style" tracking

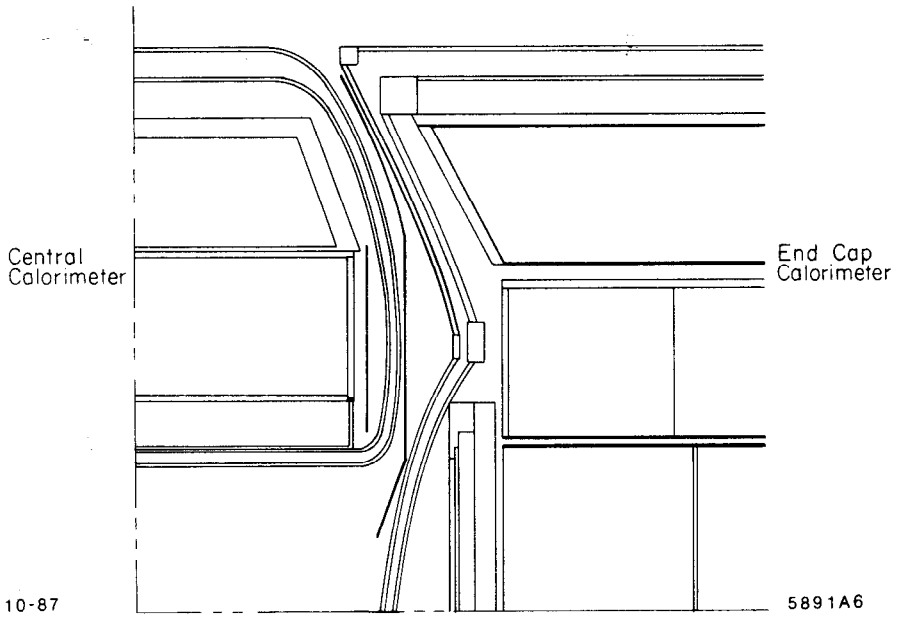

Fig. 6. D0 detector (Fermilab) central/endcap transition region.

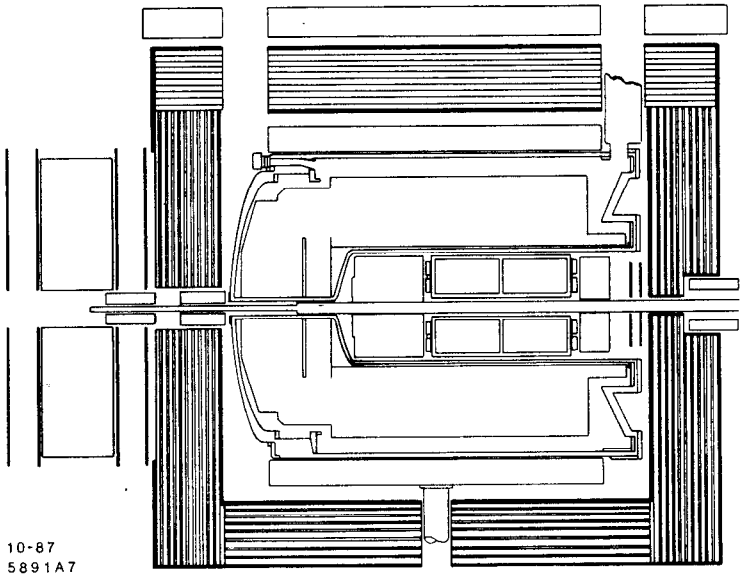

Fig. 7. H1 detector (HERA).

system. It would be built early enough to run in and debug and then buried with limited access for repairs. Given the size of the SSC calorimeters, one can even contemplate person sized access ports, judiciously placed to permit limited access to the tracker.

An alternate approach is to subdivide the argon vessels, and place them in a common

insulating vacuum vessel. This was the approach taken (for other reasons) on the Mark II liquid argon system. The vacuum vessel can be more easily flanged, and crossing from one argon vessel to another requires crossing only two walls. This approach can be continued to the point where each gap has its own liquid container, and modules then can have a vacuum vessel which uses the absorber as mechanical support. At this point the liquid argon and warm liquid systems are almost identical.

A more conservative approach would maintain completely separate vessels for the various angular regions, but would seek to optimize the placement of transition regions and the material in them. A particular approach being used in D0 attempts to incorporate the vessel wall material into the calorimetry by interspersing readout cells as frequently as possible between the walls, approaching the sampling fraction of the calorimeter itself.

The crucial question is whether liquid argon systems can be made as hermetic as any other form of calorimetry. One must compare systems after the realities of support, services and access are designed in. Given sufficient engineering and creative approaches to calorimeter segmentation and tracking access, liquid argon calorimeters are a viable option for the SSC.

4.4.2. Lead (Uranium)/Warm Liquid

The use of warm liquids in calorimetry is partly an attempt to realize the desirable features of liquid argon in a technology that does not require large cryogenic vessels with their problems of dead regions and dead materials. At the same time the hydrogen content of the warm liquids gives the potential for constructing a compensating device.

The use of warm liquids has been the subject of intense development by the UA1 collaboration who have established the high liquid purity conditions that are necessary for satisfactory operation. This involves extreme care in the preparation and cleaning of the so-called UA1 "boxes" that contain the warm liquid. The liquids themselves are now commercially available with the required purity. However, depending on the details of the system, there may be problems in sustaining this purity level over prolonged periods.

There are several factors that must be taken into account in the choice of warm liquid and its expected performance relative to that of liquid argon. The two main contenders in the choice of warm liquid are currently TMS (tetramethylsilane) and TMP (2,2,4,4-tetramethylpentane), although there are other, less well investigated, possibilities such as hexamethylethylenedisilane. The specific energy loss for minimum ionizing particles is very similar for TMS and TMP (around 2 MeV-cm^2/g) as are the free electron yields. The yields are, however, significantly smaller (by about a factor of three) than that of liquid argon. This situation can be improved somewhat by operating at high electric fields. There are also benefits in terms of increased drift velocity from high field operation. These two factors taken together can lead to signal/noise ratios for TMS and TMP equal to or better than that for liquid argon depending on the value of the field used. This occurs when fast shaping electronics is used and the signal/noise ratio is determined only by the peak current. This current is proportional to the product of the amount of liberated charge and the drift velocity. As the electric field is increased a point is reached at which

the lower charge yield of the warm liquid is compensated by the increase in drift velocity, which is faster for TMS and TMP than for liquid argon. The result is that the signal/noise ratio for TMS is equal to that for liquid argon at 25 kV/cm and the corresponding point is reached for TMP at 80 kV/cm. The price paid for this lies in the increased problem of high voltage breakdown at these high fields and is an area that needs to be studied.

The physical properties of the warm liquids lead to constraints on their use. Both TMS and TMP are highly flammable and thus have major safety problems. The use of TMS in combination with uranium is excluded because of the uranium fire hazard. However, after the recent work on the understanding of compensation, it appears to be feasible to design a compensating lead/warm liquid calorimeter thus widening the allowed choice of warm liquid. This is also important since the response time of a TMS calorimeter would be 2 to 3 times faster than a liquid argon device which would, for instance, lead to a reduction in the fake missing E_t signal from pile-up.

The use of warm liquids would also allow the possibility of putting the charge preamplifiers inside the liquid since there would be no strong restriction on their power dissipation. This gives very short cable delays and hence short signal rise times. Alternatively, the use of small modules containing warm liquid (as opposed to the large liquid argon systems) would also allow fairly short cables even if the preamps were mounted outside the modules.

One of the main original motivations for the use of warm liquids was the potential for a hermetic design. Clearly only single walls are needed to contain the warm liquid and not the double walls, with their attendant dead spaces and dead material, needed for liquid argon. Also the need to have a small number of large vessels is removed and this allows the smaller individual modules to have thinner walls. Although a careful engineering study is needed, it should be possible to support the warm modules using external braces, or, if necessary, supporting structural members could be bathed in the warm liquid since the thermal connection to the exterior is no longer a problem.

A wide variety of module shapes is possible. One possibility discussed at the Workshop would be to build "logs" of stacked thin boxes and absorber plates and then build up the calorimeter from these logs. The cracks between the logs can and should be non-projective and cables from the calorimeter and TRD/tracking system extracted at a number of distributed azimuthal locations. Even though there are still potentially troublesome cracks between the central and end sections of the calorimeter these should be much less severe than in an equivalent liquid argon design.

There should be no problem in satisfy the physics requirements of transverse segmentation since the situation is close to the well studied liquid argon case. Equally, longitudinal segmentation is achieved by the appropriate connections of the thin box layers.

The question of radiation hardness of the warm liquids is unclear. This question has to be studied in the context of whether one has a fill-and-seal system or a recirculating system for the warm liquid. A recirculating system would, apart from the obvious increase in complexity, add extra dead material in the form of pipes and manifolds. Such effects need careful modeling to be understood. While warm liquids are almost certainly not

as radiation resistant as liquid argon, it may only be necessary to provide for liquid replacement in the region of the end plug, close to the beam axis. Calculations indicate that it should be possible to build even a non-uranium warm liquid calorimeter with a hadronic energy resolution of 30 to $35\%/\sqrt{E}$ and a small constant term if the device is correctly compensating and has the potential stability of calibration and operation foreseen for such devices.[8]

4.4.3. Uranium/Silicon

The uranium/silicon design described here is an evolution of the design originally outlined at the Workshop on Physics of Future Accelerators, La Thuile.[15] Because of this previous work this design is presented in rather greater detail than the other options considered. The advantage of silicon readout for calorimetry is its potential for absolute gain calibration and stability. It also offers the chance for very fine segmentation in both transverse and longitudinal directions with correspondingly good two jet separation and lepton isolation capabilities.

The disadvantages of silicon are its high unit cost and its limited tolerance to radiation damage, compared to liquid argon or warm liquid calorimeters.

This section discusses an extension of the La Thuile work, presenting a mechanical structure, a readout scheme, and a preliminary radiation damage estimate for a very compact device aimed at excellent lepton isolation and electron/hadron separation.

4.4.3.1 Electromagnetic Section

The electromagnetic section of the calorimeter is one of the most important parts of the detector. It must identify and measure the vector momentum of all electrons in the midst of high-density hadronic flux through the same region. Therefore, good lateral and longitudinal segmentation is needed to reject hadronic interactions in the electromagnetic section, as well as to provide a strong isolation capability to tag, for example, b-jet decays.

Fig. 8 shows the electromagnetic section in detail. The cell structure uses 2-mm (0.6 radiation length) uranium plates followed by a 2-mm gap containing the silicon readout layer (0.4 mm) and its backing layer (1.6 mm G-10). The readout electronics for each layer is embedded in the backing. As at La Thuile, the cell size is 2 cm $\times$ 2 cm in the silicon. After each 5 radiation length module, there would be a silicon strip detector (x-y readout) of 0.5 mm pitch to allow determination of the shower centroid to a precision of about 0.15 mm, as well as to supply a measure of the electron angle from the shower shape asymmetry. This additional readout data adds little to the overall cost or complexity of the detector but adds greatly to the ability to resolve electrons from nearby photon showers. It makes the effective two-shower separation in the detector roughly a factor of 10 better than the 2 cm square cells by themselves. The effective segmentation for electrons of this device is approximately 0.5 $\times$ 0.5 cm at a mean radius of 64 cm. This segmentation is much finer than is needed for trigger purposes, but it gives a very powerful handle on lepton isolation in the offline analysis.

The characteristics of the electromagnetic section are given in Table 2. The barrel region is made of "logs" assembled with non-pointing cracks. The importance of ensur-

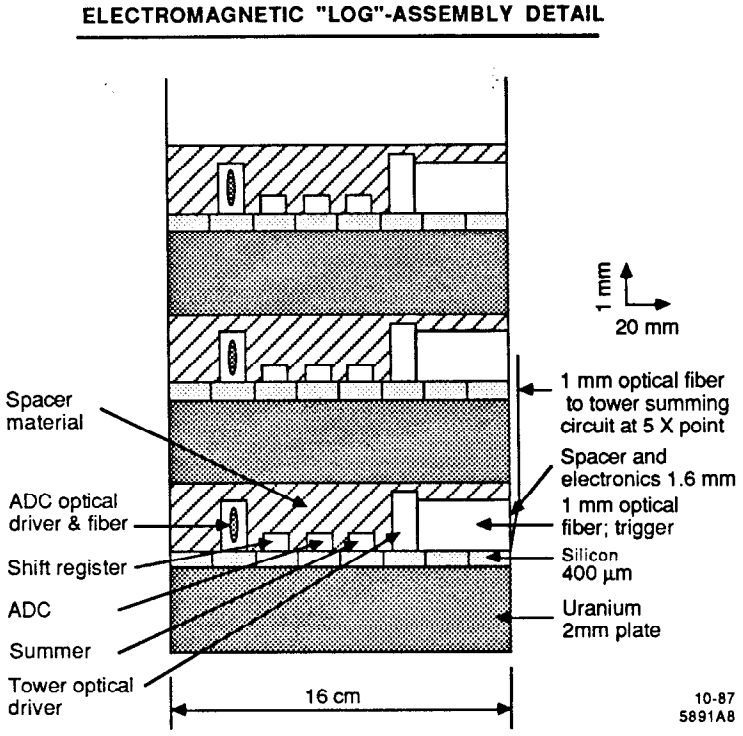

Fig. 8. Uranium/silicon calorimeter electromagnetic section detail.

ing full shower containment despite assembly breaks in the calorimeter was emphasized repeatedly at the Workshop by many people. This particular structure represents a mechanical assembly that is both practical and minimizes shower degradation. A real design will take careful engineering and physics analysis to optimize. We have imagined that the plates would remain parallel to the beam axis out to 45 degrees, then turn normal to the axis. This minimizes the effects of polar angle variations in the resolution and also makes a mechanical assembly using external support frames conceivable. Details are indicated in Fig. 9. Readout fibers from the longitudinal section would emerge in the matching region between longitudinal and vertical plates. For the endcaps, one must confront the difficult problem of a greatly-increased radiation damage rate as the distance off the beam axis is reduced. The $1/\sin\theta$ increase of $\Delta\eta$ with fixed $\Delta\theta$ in the forward direction requires a cell size in the electromagnetic towers that is not much larger than the 2 cm $\times$ 2 cm cells in the barrel region in order to maintain good electron isolation sensitivity for $\eta > 1.7$.

The question of how best to cover this forward region with good electron resolution is a very demanding one for any calorimeter technique and one for which we have no unique answer. Based on the La Thuile radiation damage calculations and the estimates of radiation tolerance given in that report, we conclude that silicon becomes unusable in the first few layers of the calorimeter for $\eta > 1.7$. This limit is soft; present studies of the question of radiation damage to silicon in a calorimeter environment will help to establish a more definite picture of the problem within the coming year . However, silicon

Table 2: Characteristics of the Uranium/Silicon Calorimeter

	Electromagnetic Section	Hadronic Section
Cell size	2 cm × 2 cm	2 cm × 2 cm
Radiator	2 mm uranium	6 mm uranium
Readout gap	2 mm	2 mm
Layers	32	132
Longitudinal sampling	5 X_0	0.5 Λ
Silicon area	300 m^2	4500 m^2
# of channels	0.75M	11.3M
Average density	9.45 g/cm^3	14.2 g/cm^3
Depth	20 X_0	8 Λ

is certain to become unusable due to radiation limits somewhere near $\eta = 2$. Can any of the radiation resistant media, in particular TMS, be made with sufficiently fine cell sizes to give good electron tags for rapidities up to 3? In order to achieve a tower size of .05 × .05 in $\Delta\eta \times \Delta\phi$, the detector element for $\eta = 2$ must be 2 cm × 2 cm in this design (z = 1.5m). At $\eta = 3$, this is reduced to 0.85 cm × 0.9 cm for the same resolution. How to achieve such small cell sizes without introducing breaks in the calorimeter structure or without extending the barrel region to such a length that there become serious weight/cost issue seems to be an important question for future SSC detector research.

We point out that a change of readout media from silicon to TMS in this sector of the calorimeter, in which plates are normal to the beam, would imply no noticeable change in detector resolution and no mechanical losses. A warm liquid device with thin container walls can be placed in the same 2 mm gap as the silicon readout. If the warm liquid has multiple plates in one liquid container, then as long as the plates are well aligned, the mechanical forces can be supported on the plates in the silicon region. From the shower resolution standpoint, if the effective radiation length of the two regions is the same, then the shower development is the same and only the cell segmentation matters for shower recognition. In U/Si or U/TMS detectors with the same gap, the radiation length is essentially identical. Therefore, one can think of mating these two different readout schemes in the transition region without sacrificing electron identification power. It may be the best way to handle this transition region.

The electronics to handle the readout for triggering and for offline analysis is discussed in the following section on readout and triggering.

4.4.3.2. Hadronic Calorimeter

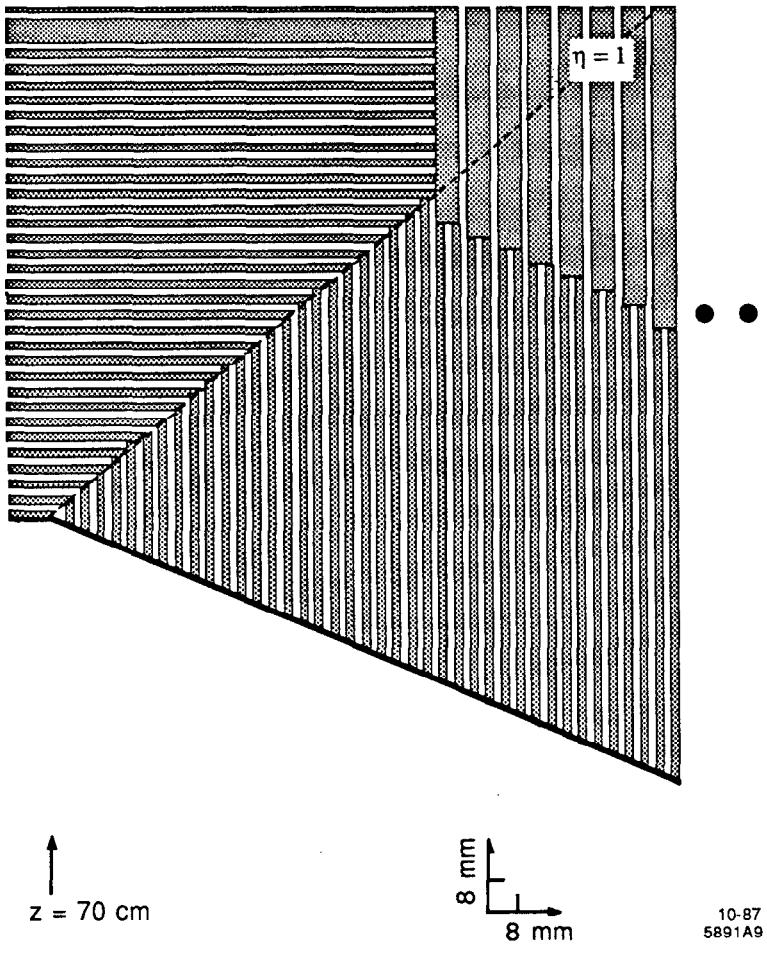

Fig. 9. Uranium/silicon electromagnetic calorimeter mechanical structure near $\theta = 45°$ where plates change orientation.

The hadronic section is built up with the same general structure as the electromagnetic section. The uranium plates are 6 mm thick, rather than 2 mm. The silicon structure is identical. The hadronic section is 8 interaction lengths deep, divided into 16 longitudinal samplings. As demonstrated in the shower resolution studies in the La Thuile proceedings, this sampling gives extremely good two-jet separation properties and will facilitate reconstructing events with W decays in the presence of other QCD background jets. The silicon required for the barrel region totals 3700 m^2.

As in the La Thuile study, this detector aims to have a balanced electromagnetic and hadronic response (e/h=1) by including polyethylene coatings as appropriate over the silicon detectors. The expected electromagnetic and hadronic resolutions should have a very small constant term. The cross-talk problem will be essentially zero, because signal processing is local and signals are converted to light directly. The anticipated resolutions, then, are $15\%/\sqrt{E}$ for the electromagnetic section and $55\%/\sqrt{E}$ for the hadronic section.

4.4.3.3. Tail Catcher

The first several layers of the muon filter include calorimeter readouts to measure energy leaking from the 8 interaction length precision calorimeter. The energy leakage will be a small fraction of the highest energy showers, so the precision of the "tail catcher" need not be great, of order $100\%/\sqrt{E}$. If gas detectors are used here, they contribute also to the muon tracking.

However, there could be problems with gaseous readouts in this region due to the neutron flux from the hadron calorimeter. Scintillator readout may be better in this regard. Such matters will be better understood as more experience is gathered from CDF.

4.4.3.4. Triggering and Readout

In a U/Si calorimeter the intrinsic segmentation is necessarily quite fine in order to keep capacitive noise suitably small. For the very fine divisions in η and ϕ mentioned earlier, the mean occupancy per silicon detector will be well below 0.1%. Hence, good zero suppression in the readout electronics is absolutely necessary. However, within a jet cone defined by $\sqrt{(\Delta\eta)^2 + (\Delta\phi)^2} = 0.4$ the particle density is quite high and many of the approximately 2000 silicon pads within this jet cone will contain energy. Thus, the readout scheme must, in a sense, cope with the worst of all situations — sparsely distributed clusters of high hit density.

Because the individual detector elements are so small and because the detector radius is also small, it seems to be a useful idea to define the tower structure of the detector in software rather than in a hardwired fashion. In order to avoid excessive cracks in the detector layout, as well as suppress capacitive noise effects, we envision doing the initial signal processing on a layer by layer basis. In this way each detector element in a given layer is available for combination with one or several elements in deeper layers to make a software-defined tower. Towers are readily modified, and tower structures can be changed in different η regions. This may be useful for special purpose studies, such as energy flow triggers or t-meson triggers.

The implementation of this idea is illustrated in the logic diagram in Fig. 10. Each detector has an on-chip preamplifier for charge/current conversion. Preamplified output signals from the 16 detectors would be loaded into a 16 channel parallel-load CCD shift register after each bunch crossing and then shifted into a 1.1 GHz flash ADC for processing. This ADC thus digitizes all the 16 detector signals in the interval between bunch crossings.

The 12-bit ADC output and 4-bit address, along with an 8-bit timing label to tag which bunch crossing out of 256 produced these data, would then go to a 2.4 GHz optical serial encoder. This encoder will not handle the high hit density that would arise from a jet between bunch crossings. One must insert a 24-bit wide by 256 bit deep 1 GHz shift register to buffer the parallel data stream coming into the serial encoder. Zero suppression is managed by imposing a digital threshold on ADC values and addresses fed into the digital delay line. In this way, the serial encoder for a given group of 16 pads sees only the average data rate over a 3.8 ms interval, rather than that from successive bursts.

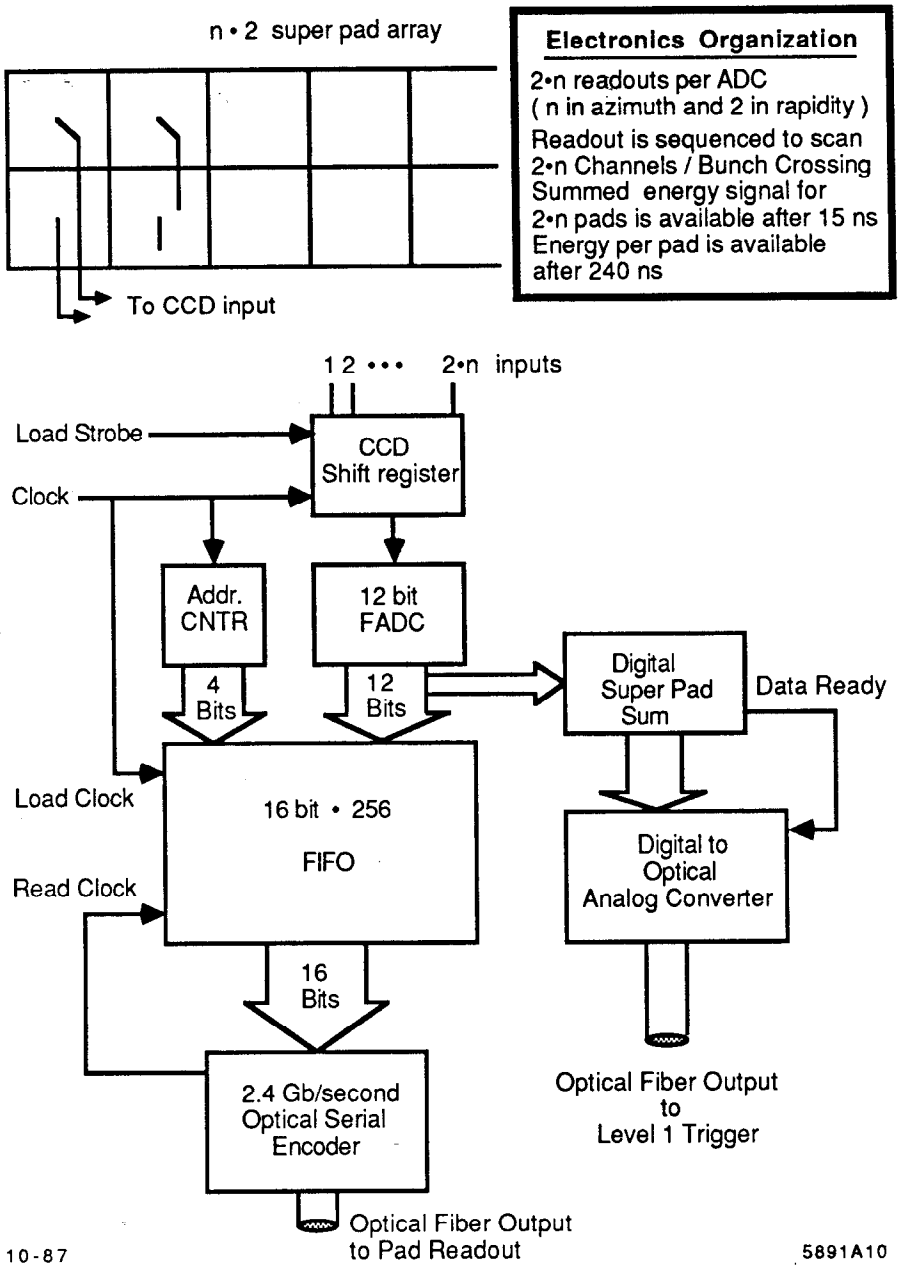

Fig. 10. Uranium/silicon calorimeter tower scheme read-out.

This shift register would have a 1GHz write clock to load data in from the ADC, but only a 40 MHz read clock to bring 24-bit words from the buffer into the serial converter input register. This kind of buffering would allow for two "full-occupancy" events, i.e., events in which all 16 detectors in one readout cluster were hit, for each 16 bunch crossings. Given the mean occupancy rate of 1.5% per crossing for any detector in the group, this seems to be sufficiently conservative to handle the design luminosity.

For trigger purposes, one must define local energy clusters. This requires summing

over many layers in this detector. One way to do this is to sum the flash ADC output, detector by detector, to form a 16-fold energy sum which would be available 30 ns after the bunch crossing. This energy sum can be converted to a light pulse in a linear fashion in a 1 GHz optical DAC and sent out on an optical fiber. Each longitudinal segment (8 per electromagnetic section, 13 per hadronic section) would be summed in depth by an electro-optic chip mounted at the end of the appropriate "log" and these energy sums combined by a microprocessor mounted in the crack at the end of the barrel to go to the level 1 trigger. Because of the high intrinsic speed of the silicon readout (charge collection <10 ns) and the immediate conversion of the energy information to an optical analog signal, this first level trigger information will be available approximately 40 ns after the event. The buffering gives adequate time to decide whether to latch the subsequent ADC information when it appears at the end of the digital buffer for conversion to serial optical data.

4.4.3.5. Mechanical Support Considerations

In the barrel region the "log" structure envisions self-contained assemblies of trapezoidal cross section with a thin stainless steel skin under tension to compress the structure and give uniform spacing. Because of non-uniformities in the exact sizes of the uranium blocks and the need for space for optical fibers and electrical power lines, we envision a 3 mm gap at the end of the barrel. A detailed sketch of this end mating is shown in Fig. 9. The brittle character of the silicon is cause for some concern about its ability to withstand the compressive loading without spacers. For the endcaps the plates are vertical, so the weight can be carried on a frame resting on the muon steel. The total weight of the barrel region is 75 metric tons, and the endcaps add 33%, for a total of 100 metric tons.

4.4.3.6. Radiation Damage Considerations

In the La Thuile study, an energy deposition study of this type of calorimeter was made. Criteria for survivability were outlined there, based on the sparse available data. Further work is now going on to develop adequate information about the lifetime of silicon detectors in calorimeter environments.

A second concern was raised with great emphasis at the Berkeley Workshop, namely, the possible damage to necessary readout electronics mounted on detectors inside the calorimeter by the flux of albedo neutrons generated in the hadronic showers. It is not clear at this time whether the readout scheme proposed here, using microprocessors and digital logic inside the calorimeter volume can be realized with sufficiently radiation-hardened devices. However, it is clear that the lifetime of readout electronics within the large detectors is a major SSC issue. The CDG has formed a task force to pursue these questions both in model studies and experiments. Answers should be available within another one or two years and will greatly affect the ultimate design of SSC detectors.

4.4.4. Lead/Scintillating Fiber

This proposed design evolved directly out of work on the understanding of the benefits of compensating calorimetry, and how to achieve compensation by varying the relative fractions of active and passive material. The basic structure is shown in Fig. 11. Plastic

fibers doped with fluor and wavelength shifter are laid in channels cut in lead sheets. Many sheets can then be stacked to build up a block. The thickness ratio of lead to fiber (about 4 to 1) is set by the requirement to obtain e/h = 1.0. This approach yields a fairly homogeneous medium and the possibility of making arbitrary shape calorimeter elements relatively easily. There may even be the possibility of constructing partially self-supporting structures from the blocks. This design overcomes the problems found in lead/scintillator sandwich designs in which one wants both thin lead plates to reduce the effect of sampling fluctuations and the correct lead/scintillator ratio for effective compensation. This leads to very thin scintillator plates which unfortunately have poor optical properties (short attenuation length). The fibers, on the other hand, have much better optical properties with attenuation lengths much longer than the effective nuclear interaction length of the lead/fiber combination. This is important for the hadronic calorimeter section since the depth profile of light production will vary from shower to shower. The problems of lateral variation in light yield across a slab of scintillator are also clearly avoided by the use of fibers.

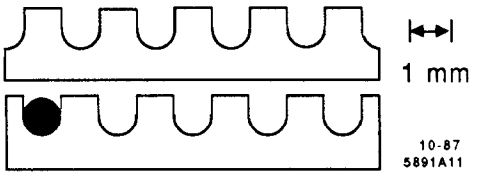

Fig. 11. Cross section of lead sheet/scintillating fiber module.

The fibers would have their axes pointing in the general direction of the interaction point, although offset by a few degrees to avoid the problem of "channeling" of particles down the fibers. There remain, however, problems associated with the finite spread of the interaction region and channeling of secondary particles produced in the calorimeter itself. More complex designs with "wiggled" fibers may offer a solution at the price of complicating the fabrication process.

The light yield of the wavelength shifter doped fibers is expected to be about an order of magnitude higher then in a system with separate scintillator and wavelength shifter. This may allow the use of solid state readout devices which would have merits in terms of calibration and stability, as well as being more compact than photomultipliers. With such a readout, longitudinal fibers and no external wavelength shifters it should be possible to achieve a design with very little dead space other that required by essential mechanical supports and signal paths to the exterior.

The attenuation induced in the fibers by radiation damage is an area of concern. It is known that, for instance, by shifting the light to longer wavelength (blue to green) it is possible to be less sensitive to the radiation damage effects. There still remain, however, unresolved issues of the effects of the large neutron flux generated in the calorimeter, and the detailed ways in which radiation of all types affects the various components of

the doped scintillating fibers. Further, until there are answers to these questions it is not possible to define with any certainty the minimum polar angle at which this type of calorimeter could operate without rapid deterioration.

One of the main practical issues in this design is how to achieve satisfactory transverse and longitudinal segmentation. The longitudinal segmentation may be achieved either by having a number of layers with fibers in each layer running the full depth of the layer, or by having groups of fibers starting at a number of different depths through a single block. The first possibility introduces more material in the form of readout devices in between the longitudinal segments which may be important for the electromagnetic section. The transverse segmentation is, however, straightforward in this option.

The second possibility leads to a serious problem of calibration since the ends of many fibers would be buried inside blocks and would be inaccessible to calibration sources. Also the transverse segmentation scheme is more complicated since it would require sums over the separately extracted longitudinal segments.

However, in both schemes there exists the possibility of choosing an almost arbitrarily fine granularity limited ultimately by the cost of the electronics for the number of channels created.

As an example we show in Fig. 12 one possible arrangement of longitudinal and transverse divisions. This example would have the fibers running the full length of each longitudinal section which in turn implies some decrease in the fiber/lead ratio with increasing radius due to the tapering of the blocks. This may not be too serious, however, since contribution to the constant term in the energy resolution is expected to be small for values of the lead/fiber ratio between 3 and 5.

Resolutions of $30\%/\sqrt{E}$ for hadrons and $15\%/\sqrt{E}$ for electrons plus a very small constant term can be obtained due to the compensated design, assuming that the contributions to the constant term from instabilities and variations across the calorimeter can be held down to low levels. These estimates will be tested in prototypes currently planned for testing in about 1 to 2 years. It should also be noted that this technique has already been successfully used on a small scale in the CERN Omega inner (electromagnetic) calorimeter.

4.5. Comparison of Techniques

While a specific recommendation for the choice of calorimeter technique for the non-magnetic detector was not made during the Workshop, there was much discussion of the relative merits of the various options. We now give a summary of the main areas of those discussions.

There was considerable concern about the survivability of detector components in the SSC high radiation environment. Only liquid argon is without potential problems in this area and can be used for all parts of a calorimeter system. The effect of radiation on warm liquids is unclear although with a fluid there always exists the option to design a recirculating, or at least a rechargeable system. The radiation hardness of silicon and

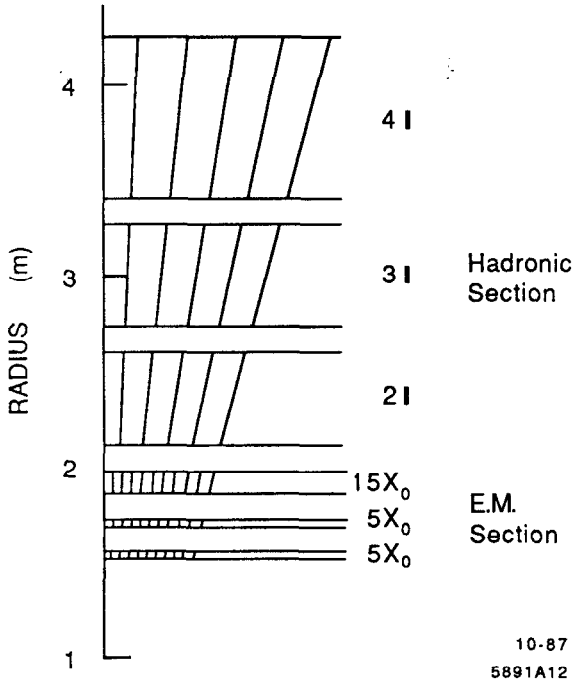

Fig. 12. Lead/scintillating fiber calorimeter segmentation.

plastic scintillating fibers is of greater concern. For silicon even "radiation hardened" versions are unlikely to be usable close to the beam axis. For the fibers there is some hope that a significant improvement in radiation hardness can be achieved with new doped scintillating materials now being developed. However, it still remains likely that there would be a change of technology in our detector in the region of 2 to 3 in η.

If such a break in the detector must occur then every effort must be made to have a smooth transition, particularly as our design aims to avoid the problems associated with a disconnected forward calorimeter section as discussed in section 4.3. In view of this, the advantages of a silicon or fiber calorimeter must be offset by the added complexity of building and operating two different types of calorimeter system. In the case of lead/scintillating fibers it was suggested that, at lower angles, it may be possible to use glass tubes containing liquid scintillator in place of the fibers. This still represents a somewhat different system, although not as fundamental as the suggested transition from uranium/silicon to warm liquid.

One problem common to all the techniques discussed arises if the amplifiers are situated on the detector. Besides the direct radiation there is expected to be a large flux of neutrons coming from the uranium or lead absorber plates. Lead may pose less of a problem but probably by less than an order of magnitude in neutron flux. The tolerance level of standard electronics to these neutrons is unclear. While it may be possible to consider radiation hardened electronics this would almost certainly increase the cost of the calorimeter.

The issue of hermeticity has already been the subject of much discussion and is one of the principal reasons why liquid argon is not the automatic choice for the SSC. An imaginative design of a unified cryostat system could go a long way towards solving the problem. However, there is still the problem that a significant amount of energy from the very soft component of jets can be lost in the walls. Warm liquids systems represent an improvement in this area, but their performance needs to be studied with a detailed simulation. The uranium/silicon and lead/scintillating fiber options are potentially very hermetic over the η range where they can be used. Care must be taken not to spoil this at the interface with the low angle system.

There is a clear advantage to be gained in speed of response by using silicon or fibers. The reduction in resolving time relative to liquid argon should give a significant improvement in the fake missing E_t situation. The situation for warm liquids is closer to that for liquid argon than the intrinsically fast fibers and silicon. At Snowmass 86 it was suggested that it may be possible for systems with slower resolving time to arrange to flag the beam crossing for towers with more than a few GeV of energy.[16] Even if this were possible there still remains the problem of unscrambling towers shared by events from different crossings.

In terms of energy resolution, the four techniques considered should all be capable of giving the required $0.5/\sqrt{E}$. Comparisons therefore focus on the constant term. With the possible exception of liquid argon it is predicted that it should be possible to design for e/h = 1.0, thus essentially eliminating one component of the constant term. The remainder of this term is driven by the stability of the calorimeter, its uniformity, and how well it can be calibrated.

Since the $\sqrt{E}$ term becomes less important at high energies, these factors must receive close attention. Good calibration and stability is indicated for all options except lead/scintillating fibers where the case has yet to be proved. There are also concerns for both the silicon and fiber systems if their performance is subject to change due to a measurable amount of radiation damage over the lifetime of the calorimeter.

The required segmentation, both transverse and longitudinal, seems no problem except in the lead/scintillating fiber case where a viable scheme has yet to be worked out in detail.

Finally, the cost of implementing the calorimeter in any of the four schemes should not be very different except perhaps in the case of the silicon where the unit cost for very large quantities needs clarification.

4.6. Questions and R&D Topics

We conclude by listing for each option the areas of concern for the focus of future R&D:

(a) Lead (uranium)/liquid argon

- cryostat design — needs an engineering study to look at the feasibility of a unified design.

- resolving time — increasing drift velocity
- electronics for event separation
- amplifier location, cable lengths
- how to make e/h closer to 1.0 (additives?)

(*b*) Lead (uranium)/warm liquids

- resolving time
- box design and dead material
- high field operation — breakdown problems
- maintaining purity in a large system
- effects of radiation on liquids and/or scheme for liquid replacement

(*c*) Uranium/silicon

- radiation effects
- silicon costs for large scale production

(*d*) Lead/scintillating fibers

- radiation effects
- liquid scintillator in glass tubes?
- practical longitudinal segmentation scheme(s)
- calibration scheme
- fiber orientation — channeling effects

(*e*) General

- support structures
- engineering breaks in technology
- use of radiation hard electronics

5. Muon Detection

5.1. Rationale for Muon Coverage and Resolution

Among the items studied by the muon subgroup were the importance of lepton coverage at small angles and the effects of muon resolution. Our conclusions are that muon coverage below 5° provides only marginal improvement in the physics capabilities and that, except for a few cases, muon momentum resolution of 10% is acceptable provided that it remains "reasonable" (less than 30%) to p_t's of ~ 2 TeV/c.

The necessary lepton coverage for high-p_t events has been discussed previously[17] and coverage down to 5° ($\eta \approx 3$) appeared sufficient. In the case of heavy Higgs production, an even smaller pseudorapidity cut would be made to increase the signal-to-background

rate compared to the Z-pair continuum.[18] For new heavy Z production, the desire to measure forward-backward asymmetries requires good acceptance at high η of the Z.[19] In Fig. 13, the acceptance is shown as a function of the rapidity of the Z for events with muons having angles $\geq 5°$ and a Z mass of 1 TeV. The total geometric acceptance is about 90% and is about 50% at the highest η(Z).

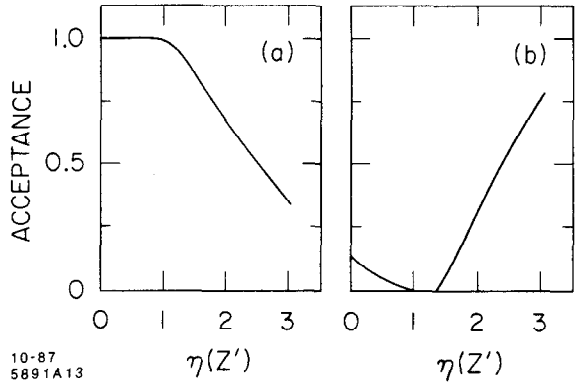

Fig. 13. The geometric acceptance versus η(Z) for a new Z with mass 1 TeV for a) a minimum angle of 5° on both leptons from $Z \rightarrow ll$ and b) requiring both leptons to be in the interval from $2.5° \leq \theta_l \leq 25°$.

Another argument which has been advanced in support of extended lepton coverage is that these muons signal the presence of neutrinos in events having missing p_t. Two cases were examined at this workshop. In the first the production and leptonic decay of the W ($W \rightarrow \mu\nu$) with $p_{tw} > 100$ GeV/c was examined. For a minimum angle of 5°, in 16% of the events the muon would not be accepted and of these, 40% would have a missing $p_t >$ 100 GeV/c (assuming perfect calorimeter coverage for $\eta \leq 5$). The contribution of these events to a missing-p_t sample is small compared to the ineradicable contribution from $W \rightarrow \tau\nu$ and $Z \rightarrow \nu\nu$ and therefore the gain obtained from extending the muon coverage below 5° would be of doubtful value.

Events containing Z + jet having $p_{tz} > 100$ GeV/c formed the second class of events with missing energy. These events are background to $H^0 \rightarrow ZZ \rightarrow ll\nu\nu$. A sample of 135,000 Z + jet events was generated using ISAJET with top masses in the range 30-85 GeV (the results were independent of the value of the top mass). As above, an almost perfect calorimeter was assumed and therefore events with missing p_t greater than 50 GeV/c were almost exclusively due to semileptonic decays of heavy quarks. The identification of extra leptons in an event would signal these quark decays. If only muons with $p_t > 10$ GeV/c and $\theta > 5°$ could be identified, then 25% of the events would be so flagged. This efficiency improved only slightly to 28% when the muon coverage was extended to 2°. A much improved efficiency could be obtained by reducing the muon p_t selection to 5 GeV/c (32%) or by the identification of both extra electrons and muons (53%). If both these selections were made 69% of the Z + jet events would be identified.

So again, additional muon coverage at small angles results in only a marginal improvement in background rejection.

Muon momentum analysis will effect the physics capability in a number of ways. The measurement of the width of a new Z depends on the resolution, but for this the electron channel will probably always be superior to the muon. Also, as Rosner has pointed out in Ref. 19, asymmetries in new Z production are not only a function of the rapidity of the Z but can also depend on the lepton-lepton mass through interference with the standard Z. Since the muon charge can be determined up to large p_t, it is the natural channel in which these asymmetries can be examined. For a 1 TeV Z, a mass resolution of 100 GeV may not be adequate to measure the asymmetries. A exhaustive study of this has not been done, but it would appear that a 25-50 GeV mass resolution at large η(Z) would suffice. A possible upgrade to the muon detector should a new Z be discovered would be to increase the iron thickness in the 2.5° to 25° region from 4 m to 12 m. The η(Z) acceptance for both leptons to be in this angular region is shown in Fig. 13. The momentum resolution for these muons will be about 5 to 8% with a corresponding mass resolution at 1 TeV of about 40 GeV.

Many high-p_t objects, such as the Higgs, will not have narrow widths. Even so, muon momentum resolution is an important consideration in the measurement of these events. Among the possible effects of poor momentum resolution are an increase in background due to the dimuons produced in $Z \rightarrow \mu\mu$ and a dilution in the ability to determine the polarization of W's or Z's arising from the Higgs decay. Only the first topic was studied during this workshop.

The predominant source of dimuon backgrounds is due to decay of heavy quarks. A heavy top decaying to W's and b's would be a great source of high-p_t muons. However, when we look at the Higgs decaying into Z's, with the Z's in turn decaying to muons, all four muons are well isolated. Imposing isolation cuts on the top events reduces that background to negligible levels simply because only a small fraction of the b decays have an isolated muon. The ability to impose these isolation cuts is clearly crucial and finely segmented calorimetry is indispensable. For the subsequent discussions we will assume that the calorimeter is segmented at least into cells of 0.1 in $\Delta\phi$ by 0.1 in $\Delta\eta$. We define a muon to be isolated if the sum of the transverse energy in the cells surrounding the one intersected by the muon plus that of the intersected cell is less than 2 GeV (a total of 9 cells). The only process we could find that could generate four isolated muons in significant numbers to be a potential background to a Higgs signal is the scenario involving a heavy fourth generation quark ($\approx$200 GeV) decaying to a heavy top ($\approx$100 GeV). If the heavy quark then decays via W + t and the top via W + b, pair production of these heavy quarks will produce events with four W's. The cross section for producing such heavy quark pairs is 4000 pb compared to the standard cross section of 4 pb for production of a 400 GeV Higgs. However, for this process the cross section for a 400 GeV Higgs is boosted to 40 pb (because of the coupling to the heavy quarks), so the background is less fierce than it might appear at first glance.

To study the importance of these heavy quark backgrounds for a Higgs signal we

generated events for a 400 GeV Higgs and 200 GeV fourth generation b quark using ISAJET. Events were retained if they had four isolated muons (according to the above criteria) with $p_t > 30$ GeV. For an integrated luminosity of 10,000 pb^{-1} we are left with 3000 background and 80 signal events. Looking at the Z's from the Higgs events we find that, for 10% rms muon momentum resolution, the full-width half-maximum Z mass resolution is 14 MeV. If we then select events with 2 distinct opposite-sign μ pairs in the mass range 82 to 106 GeV, we are left with 60 signal and 100 background events. The invariant mass of the ZZ pair, however, peaks below 300 GeV for the background events. If we further select those events with the ZZ effective mass in the range 350 to 450 GeV, we have 50 signal/15 background events. Note that the four muon final state is the worst possible case. The inclusion of events with electron pairs will reduce the background because of the better electron energy resolution and the reduction of the combinatorial background.

In conclusion, although a heavy fourth generation quark could generate non-negligible backgrounds to a purely leptonic Higgs signal, the signal-to-background ratio is expected to be good enough so that it is not a serious problem. Muon momentum resolutions of better than 10% are not required, but, if the resolution were to get worse by a factor of 2, the signal-to-background ratio in the 4-muon final state would deteriorate from 10/3 to 5/6.

5.2. Muon Detector

The apparatus needed to identify and measure the muon is shown schematically in Fig. 1. Three meters of iron are arranged in roughly cylindrical shapes just outside the calorimeter. At each end are seven annular disks about the beam. The entire spectrometer is magnetized such that there is a toroidal magnetic field of 1.8 T in each iron section (of course, the field approaches 2.0 T near the inner radii of the disks).

The environment outside of the calorimeter is assumed to be quiet enough to allow the use of drift chambers. The choice of drift distance is clearly dependent on the noise rate and the readout cost. The chambers are presumed to have a 70 μm point resolution and have some vector capability as well. The inner chambers are presumed to measure the direction of the muon incident on the iron to an accuracy of 0.5 mrad. This is a significant requirement but can be achieved by measuring several points to a precision of 70 μm over 30 cm. Similarly, the muon direction is also measured after exiting the iron to the same accuracy. (The gain in resolution in measuring the exit angle much better is marginal unless the muon track can be identified in the central tracking device.) In addition there are scintillation counters deployed as shown which can be used in the trigger and to tag the particular bunch crossing. They also provide the time reference for the drift chambers.

The geometry is chosen so that a muon will traverse $\geq$ 5.4 Tm for $\theta \geq 28°$ and 7.2 Tm for $5° < \theta < 28°$. The fractional momentum resolution is calculated assuming point measurements of 70 μm accuracy between the iron segments and adjacent to each outer side, and independent angle measurements both before and after the iron to an accuracy

of 0.5 mrad. The resolution is obtained from a calculation[20] including measurement errors and multiple coulomb scattering and is shown in Fig. 14 for the different paths (no allowance for the increase in path due to oblique incidence is made).

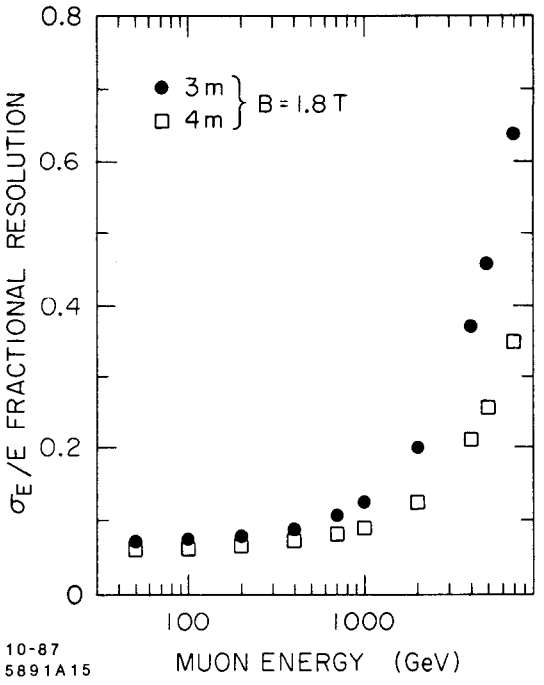

Fig. 14. The resolution of the muon spectrometer as a function of momentum. The muon traverses 3 m of magnetized iron for angles greater than 28° and for angles less than 28° and greater than 5° it traverses 4 m. Chamber resolutions are as noted in the text.

5.3. Muon Trigger Rates

The muon trigger rates for a generic SSC detector were calculated during Snowmass 86 and are given in the Muon Detector Group Report.[21] The geometry assumed was similar to that envisioned for the non-magnetic detector with precisely the same number of calorimeter absorption lengths and lengths of magnetized iron. The central detector was assumed to be a cylinder 5 m long with a 2.5 m radius (i.e. shorter but thicker then for the non-magnetic design). The size of the central detector affects the π/K decay rate. The trigger rate is dominated by decays at small angles and low p_t (below 15 GeV/c), but these decays make an almost negligible contribution to higher p_t single muon rates or to dimuon rates. For now, we will ignore the small differences in geometry and just summarize the Snowmass 86 numbers.

At the standard luminosity, the raw muon rates for angles greater than 5° will be about 300 kHz. In order to lower the rate to 1 Hz, one will have to impose a p_t cut of about 100 GeV/c. Most of the muons are in the forward region with only about a 10 kHz

rate for angles greater than 20°. The dimuon rate is much lower with only a 1 kHz rate for no p_t cut and a 10 Hz rate if both muons are required to be have p_t greater than 25 GeV/c.

As an example of a triggering scheme, we examine the QCD rates for a W trigger. A first level cut of $p_t \geq 25$ GeV/c using only muon hits reduces the rate from 300 kHz to 600 Hz. If at this point we assume we have a crude missing-p_t vector, then a loose m_t cut between 35 and 120 will further reduce the rate to 20 Hz. Finally, an isolation cut on the muon will reduce the rate by about two orders of magnitude (it may be preferable to apply this isolation cut before the m_t cut). These criteria will reduce the $W \rightarrow \mu$ trigger rate from QCD sources to well below the approximately 10 Hz rate from $W \rightarrow \mu\nu$. Further selection must be made on the detailed physics of the event, *i.e.*, the p_t of the W, or other characteristics of the events.

To date the design of the muon trigger hardware is conceptual at best. It is believed necessary to install trigger counters (probably two layers outside the iron) to quickly and precisely determine which bunch has produced the muon. These counters would also be used as a level 0 muon trigger with the 300 kHz rate mentioned above. D0 is currently envisioning using a similar counter array as a muon trigger for high luminosity and will also add a 300 ns lumped delay at the front end of its muon electronics.[22] With this, they believe that other pipelining will not be necessary for the muon data.

6. Trigger

A major problem for any 4π SSC detector is how to reduce the 60 Mhz interaction rate to an approximate trigger rate of 1 Hz. We have discussed some aspects of triggering in previous sections (4.4.3.4 and 5.3); here we give a brief overview of a generalized trigger which would be tailored to the specific adopted technologies.

The trigger would contain four levels, each reducing the rate by approximately two orders of magnitude. The zeroth level would be a deadtimeless pre-trigger which works on pipelined signals from the calorimeter towers. Sums of electromagnetic and hadronic energy in $\Delta\eta \times \Delta\phi$ bins of 0.1×0.1 would be formed, and transverse energy cuts would be made at around 20 to 30 GeV. This trigger would probably take between 500 ns and 1 μs, requiring a pipeline of this length.

The level 1 and 2 triggers together would reduce the rate from about 1 MHz to about 100 Hz. They would do this by applying increasingly sophisticated analyses to the calorimeter data and by integrating information from the muon trigger (see Section 5.3). Isolation cuts and topology cuts could be applied at these levels.

The final level of trigger would be done by microprocessor farms doing a preliminary analysis of the entire event.

7. Detector Cost

We have estimated the cost of the non-magnetic detector using the cost schedule established by the SSC Detector Cost Evaluation Panel[23] The result is shown in Table 3. We note that the total, 193 M$, is about two-thirds of the cost estimated for a large solenoidal detector.[23]

Table 3: Detector Cost Estimates

Item	Number	Units	Cost (M$)
Tracking & TRD's			
Mechanical	330	k wires	33.0
Electronics	340	k channels	40.8
Calorimeter			
Precision mechanical	1600	tons	25.6
Catcher mechanical	1500	tons	5.2
Electronics	200	k channels	24.8
Muon system			
Toroids	10500	tons	12.6
Chambers	3700	m^2	7.4
Electronics	120	k channels	12.2
Computing	1	system	5.0
EDIA	20%		32.2
Total			**193.0**

8. Conclusions

We have presented a model of a detector that meets all of the major requirements given to us by the physics parameters groups.

By employing a combination of track-matching, calorimetric longitudinal and transverse shower profile measurements, and TRD information, the detector is capable of superior electron identification. It has an excellent muon identification and measurement system. And it allows the use of an optimized calorimeter that is not compromised by the requirements of a large magnetic field.

Thus, we conclude that a "non-magnetic" detector is a strong candidate for a 4π SSC detector for the study of high-mass phenomena.

Acknowledgement

We are indebted to V. Chernjatin, B. Dolgoshein, and J. Schukraft for information on TRD design considerations and performance that has been included in this report.

References

1. C. Fabjan, in *Experimental Techniques in High Energy Physics,* T. Ferbel, ed., Addison-Wesley, 1987; Y. Fukui *el al.*, *Proceedings of the Summer Study on the Physics of the Superconducting Supercollider,* Snowmass 1986, p. 417.
2. R. DeSalvo, *Proceedings of the 1986 Summer Study on the Physics of the Superconducting Supercollider,* June 23–July 11, 1986, Snowmass, Colorado, p. 391; A. Odian, *ibid.,* p. 398.
3. B. Dolgoshein, *Nucl. Instrum. Methods* **A252**, 137 (1986).
4. S. P. Swordy *el al.*, *Nucl. Instrum. Methods* **193**, 591 (1982); H.-J. Butt *el al.*, *Nucl. Instrum. Methods* **A252**, 483 (1986).
5. J. Beatty, private communication.
6. F. E. Paige and S. D. Protopopescu, BNL-38034 (1986).
7. A. H. Walenta, *Nucl. Instrum. Methods* **217**, 65 (1983).
8. R. Wigmans, *Nucl. Instrum. Methods* **A259**, 389 (1987).
9. B. Pope, *Physics at the Superconducting Super Collider Summary Report,* Fermilab, June 1984.
10. R. Wigmans, these proceedings.
11. T. Kondo *el al.*and J. Huston *el al.*, *Proceedings of the 1984 Summer Study on the Design and Utilization of the Superconducting Super Collider,* June 23–July 13, 1984, Snowmass, Colorado.
12. H. Gordon and P. Grannis, *Proceedings of the 1986 Summer Study on the Physics of the Superconducting Supercollider,* June 23–July 11, 1986, Snowmass, Colorado.
13. A. Jonckheere, D0 internal note.
14. H1 Detector Design Report.
15. *Proceedings of the Workshop on Physics at Future Accelerators,* La Thuile, Val d'Aosta, Italy, CERN 87-07.
16. C. Baltay, J. Huston, B. Pope, *Proceedings of the 1984 Summer Study on the Design and Utilization of the Superconducting Super Collider,* June 23–July 13, 1984, Snowmass, Colorado.
17. D. Carlsmith, D. Hedin and B. Milliken, *Proceedings of the 1986 Summer Study on the Physics of the Superconducting Supercollider,* June 23–July 11, 1986, Snowmass, Colorado, p. 431.
18. Report of the Heavy Higgs Group, these proceedings.

19. J. L. Rosner, *Proceedings of the 1986 Summer Study on the Physics of the Superconducting Supercollider,* June 23–July 11, 1986, Snowmass, Colorado, p. 213.

20. C. Zupancic, CERN/EP/NA4 Note 81-8 (unpublished) and C. Zupancic (to be published)

21. D. Carlsmith *el al.*, *Proceedings of the 1986 Summer Study on the Physics of the Superconducting Supercollider,* June 23–July 11, 1986, Snowmass, Colorado, p. 405.

22. D. Green, D0 Note 557, Fermilab, 1987.

23. SSC Central Design Group, SSC-SR-1023 (1986).